

Thermal quench of a dynamical QCD model in an external electric field

S. Heshmatian^{a1} and A. Trounev^{b2}

^a *Department of Engineering Sciences and Physics, Buein Zahra Technical University, Buein Zahra, Qazvin, Iran*

^b *Department of Computer Technology and Systems, Kuban State Agrarian University, Krasnodar, Russia*

In this article, we investigate the thermal equilibration of the holographic QCD model dual to the Einstein-Maxwell-Dilaton (EMD) gravity in the presence of an external electric field. The model captures the QCD features at finite temperature and finite chemical potential in both confinement and deconfinement phases and could be considered a good candidate to study the dynamics of the strongly interacting system in out-of-equilibrium conditions. For this purpose, we examine the instability imposed by an external electric field using the AdS/CFT dictionary and study the electric current flow and its relaxation for this holographic model. We study the effects of temperature, electric field strength, and chemical potential on the current flow of the stationary state by applying a constant electric field. Additionally, for a time-dependent electric field, we investigate the relaxation time scales of the system using equilibration time and thermalization time. Finally, we compare our results with those from other holographic models and experiments.

¹e-mail:heshmatian@bzte.ac.ir

²e-mail:trounev.a@edu.kubsau.ru

Contents

1	Introduction	1
2	Einstein–Maxwell-dilaton model	3
3	Stationary current	8
4	Time dependent current	11
5	Conclusion	16

1 Introduction

Gauge/gravity duality serves as a powerful tool for exploring out-of-equilibrium strongly coupled systems. The original duality establishes a correspondence between the $\mathcal{N} = 4$ super Yang-Mills theory and Type IIB string theory in $AdS_5 \times S^5$, and serves as a powerful tool to investigate the gauge theory at large N_c and strong coupling [1]-[5]. However, given that the physical quantities in Quantum Chromodynamics (QCD) are temperature-dependent, significant efforts have been undertaken to extend this duality and develop more realistic holographic models capable of representing real-world QCD phenomena [6]-[19]. As perturbative QCD is only valid in the weak coupling regime and lattice QCD techniques are suitable for equilibrium conditions, the adoption of holographic QCD models has become prevalent to capture the behavior of strongly coupled dynamic systems.

Investigating the instabilities of the quark-gluon plasma (QGP) under the external electric fields is an interesting research subject, as experiments suggest the presence of strong electromagnetic fields after the QGP formation, which might influence the medium around the phase transition temperature [46],[74]. These strong electric fields could potentially lead to the creation of quark-antiquark pairs, analogous to the QED Schwinger effect where electron-positron pairs are created via the vacuum decay in the presence of an external electric field [48],[49]. In the AdS/CFT context, this effect was initially explored by considering a rectangular or circular Wilson loop and calculating the quark-antiquark potential [50] and subsequently in [51]-[61]. An alternative approach is the Hashimoto-Oka method [40] which associates vacuum instability with the imaginary part of the effective action for the flavor probe brane.

The time evolution of a strongly coupled gauge theory system at a finite temperature is an interesting dynamical process investigated using the AdS/CFT correspondence. The system evolves from an initial Hamiltonian H_0 to the final state of a modified Hamiltonian due to the energy injection in a time interval. As the initial state is at non-zero temperature, this process is called the *thermal quench*. This is a dynamic time-dependent process, and the system evolution is controlled by a characteristic time scale determining the energy injection rate [29]-[35]. If the energy is injected via an external electric field, the gauge field is mapped to an electric current in the boundary theory [36]-[40] and applying a time-

varying electric field, gives rise to a time-dependent current flow, which eventually settles into its steady state [40]-[45].

Quark-gluon plasma produced at RHIC and LHC experiments, is a strongly interacting system with rapid thermalization. The thermalization time of heavy quarks has been estimated using the lattice QCD [20]-[21] and also using the elliptic flow data at RHIC by the hydrodynamics simulation which is shown to have an upper limit of order $1\text{fm}/c$ [22]. It could be obtained using the Langevin dynamics and Boltzmann transport approach to calculate the spatial diffusion coefficient, which is a crucial transport parameter related to the elliptic flow v_2 in heavy-ion collisions, which leads to a thermalization time in the range $4 - 6\text{fm}/c$ for temperatures in the range $T_c - 3T_c$ with $T_c \simeq 155\text{MeV}$ [23]-[24]. The thermalization time of a heavy quark is also estimated based on the leading order perturbative QCD for constant and running couplings in [25]-[26] where much larger values for the heavy quark thermalization time have been estimated compared to the Langevin dynamics and Boltzmann transport approach.

Also, many attempts have been made to study various time scales of the quark-gluon plasma in the context of the AdS/CFT correspondence. For example, using the spatial diffusion coefficient, the thermalization time has been shown to scale as $1/T^2$ which leads to a relaxation time of roughly $2\text{fm}/c$ for charm quarks at $T = 250\text{MeV}$ [27]. Furthermore, a universal lower bound for the thermalization time of a massless hypermultiplet in the presence of an external electric field has been suggested to be roughly $1\text{fm}/c$ in the Hashimoto-Oka model [40]. Also, the isotropization time in far-from-equilibrium non-isotropic plasma has been studied using a time-dependent shear in the geometry and found the isotropization time to be of order $0.5\text{fm}/c$ in Ref. [28].

On the other hand, the confinement-deconfinement phase transition is an intriguing phenomenon of QCD that leads to the dissociation of quarkonium bound states near the phase transition temperature, as confirmed by the experimental findings [63],[64]. This suppression of quarkonium is more prominent at low energy densities, with the confined phase residing at lower temperatures and densities while the deconfined phase exists at higher temperatures and densities. Extensive theoretical studies have been performed to describe this phenomenon. Notably, lattice QCD calculations of the entropy of quark-antiquark pairs exhibit a peak near the phase transition region, indicating strong interactions [65]. To model the QCD confinement-deconfinement phase transition, a holographic QCD model has been proposed in [66] based on the Einstein-Maxwell-dilaton gravity model. This model provides a realistic framework for the QCD confinement-deconfinement phase transition with thermodynamic properties consistent with QCD and lattice results. The gravitational solution is at a finite temperature and indicates a first-order Hawking/Page phase transition from thermal-AdS to a black hole on the gravity side, corresponding to the standard confinement/deconfinement phases in the dual QCD theory. Furthermore, the model includes chemical potential, as the QCD confinement-deconfinement critical temperature and equation of state are sensitive to the chemical potential.

Motivated by the above contents, we are going to study the thermal quench of the holographic model [66] in the presence of external electric fields. For this purpose, we employ the case of standard confinement-deconfinement phase transition of the holographic

model and consider two cases of constant and time-dependent applied electric fields. In the case of a constant external electric field, we calculate the stationary current in terms of temperature and electric field strength for different charge densities and chemical potential values. For the time-dependent case, the electric field is considered such that it starts from zero and reaches its final value. In this case, we determine the equilibration time for the thermal quench which is defined as the time when the time-dependent current approaches its final stationary value with 5% uncertainty and stays in this regime afterward. The equilibration time dependency on the electric field and chemical potential is calculated numerically for a constant quench speed. Additionally, we examine the system's response in both fast and slow quench regimes, specified by small and large values of the characteristic time scale. For the fast quench regime, which corresponds to the small characteristic time scales, the universal behavior of the thermal quench is demonstrated. The rescaled equilibration time indicates an adiabatic behavior for the slow quench regime corresponding to the large characteristic time scales. Also, we study the thermalization time for the holographic QCD model which is the time for the apparent horizon to approach the event horizon given by $z = zp$ on the probe brane. This means that, in the dual boundary theory, the boundary current approaches its final steady-state value corresponding to the electric field's final value.

The organization of the paper is as follows: In section 2, a brief review of the standard confinement/deconfinement phase transition of the Einstein-Maxwell-dilaton model of [66] is presented. In section 3, the stationary current flow of this dynamical holographic QCD model in the presence of a constant external electric field is studied in terms of the electric field strength and temperature for different chemical potential and charge density values. In section 4, the response of the holographic model to a time-dependent electric field is investigated in terms of the electric field strength, temperature, and chemical potential values. Also, this dynamical process is studied in the fast quench and slow quench regimes in terms of the characteristic time scale k . Finally, we summarize our results in section 5.

2 Einstein–Maxwell-dilaton model

In this section, we briefly review the holographic QCD model of [66] constructed from the Einstein-Maxwell-dilaton gravity model.

The Einstein-Maxwell-dilaton action in five dimensions is,

$$S_{EM} = -\frac{1}{16\pi G_5} \int d^5x \sqrt{-g} \left[R - \frac{f(\phi)}{4} F_{MN} F^{MN} - \frac{1}{2} \partial_M \phi \partial^M \phi - V(\phi) \right]. \quad (2.1)$$

In this equation, $V(\phi)$ is the dilaton field potential, $f(\phi)$ is a gauge kinetic function representing the coupling between dilaton and gauge field A_M , and G_5 is the Newton constant. From the above action, the Einstein, Maxwell, and dilaton equations of motion could be obtained as,

$$R_{MN} - \frac{1}{2} g_{MN} R - T_{MN} = 0, \quad (2.2)$$

$$\nabla_M [f(\phi)F^{MN}] = 0, \quad (2.3)$$

$$\partial_M [\sqrt{-g}\partial^M\phi] - \sqrt{-g}\left(\frac{\partial V}{\partial\phi} + \frac{F^2}{4}\frac{\partial f}{\partial\phi}\right) = 0 \quad (2.4)$$

where

$$T_{MN} = \frac{1}{2}\left(\partial_M\phi\partial_N\phi - \frac{1}{2}g_{MN}(\partial\phi)^2 - g_{MN}V(\phi)\right) + \frac{f(\phi)}{2}\left(F_{MP}F_N{}^P - \frac{1}{4}g_{MN}F^2\right).$$

By considering the following ansatz for the metric, gauge field, and dilaton field,

$$ds^2 = \frac{L^2 e^{2A(z)}}{z^2} \left(-g(z)dt^2 + \frac{dz^2}{g(z)} + dy_1^2 + dy_2^2 + dy_3^2 \right),$$

$$A_M = A_t(z), \quad \phi = \phi(z), \quad (2.5)$$

the eqs. (2.2), (2.3) and (2.4) could be solved simultaneously to obtain the following equations,

$$\phi'' + \phi' \left(-\frac{3}{z} + \frac{g'}{g} + 3A' \right) - \frac{L^2 e^{2A}}{z^2 g} \frac{\partial V}{\partial\phi} + \frac{z^2 e^{-2A} A_t'^2}{2L^2 g} \frac{\partial f}{\partial\phi} = 0, \quad (2.6)$$

$$A_t'' + A_t' \left(-\frac{1}{z} + \frac{f'}{f} + A' \right) = 0, \quad (2.7)$$

$$g'' + g' \left(-\frac{3}{z} + 3A' \right) - \frac{e^{-2A} A_t'^2 z^2 f}{L^2} = 0, \quad (2.8)$$

$$A'' + \frac{g''}{6g} + A' \left(-\frac{6}{z} + \frac{3g'}{2g} \right) - \frac{1}{z} \left(-\frac{4}{z} + \frac{3g'}{2g} \right) + 3A'^2 + \frac{L^2 e^{2A} V}{3z^2 g} = 0, \quad (2.9)$$

$$A'' - A' \left(-\frac{2}{z} + A' \right) + \frac{\phi'^2}{6} = 0 \quad (2.10)$$

Here, it is assumed that various fields depend only on the extra radial coordinate z . Also, $z = 0$ corresponds to the asymptotic boundary of the spacetime and L is the AdS length scale. Out of these differential equations, it is consistent to consider only four equations and the eq. (2.6) is considered as a constraint equation. Subsequently, other equations could be solved analytically in terms of functions $A(z)$ and $f(z)$ as,

$$g(z) = 1 - \frac{\int_0^z dx x^3 e^{-3A(x)} \int_{x_c}^x dx_1 \frac{x_1 e^{-A(x_1)}}{f(x_1)}}{\int_0^{z_h} dx x^3 e^{-3A(x)} \int_{x_c}^x dx_1 \frac{x_1 e^{-A(x_1)}}{f(x_1)}},$$

$$\phi'(z) = \sqrt{6(A'^2 - A'' - 2A'/z)},$$

$$A_t(z) = \sqrt{\frac{-1}{\int_0^{z_h} dx x^3 e^{-3A(x)} \int_{x_c}^x dx_1 \frac{x_1 e^{-A(x_1)}}{f(x_1)}}} \int_{z_h}^z dx \frac{x e^{-A(x)}}{f(x)},$$

$$V(z) = -\frac{3z^2 g e^{-2A}}{L^2} \left[A'' + A'(3A' - \frac{6}{z} + \frac{3g'}{2g}) - \frac{1}{z} \left(-\frac{4}{z} + \frac{3g'}{2g} \right) + \frac{g''}{6g} \right] \quad (2.11)$$

Here, the boundary condition is considered such that $g(z_h) = 0$ at the horizon and $g(z) \rightarrow 1$ at the asymptotic boundary. The integration constant x_c in eq. (2.11) is fixed in terms of the chemical potential of the boundary theory. Chemical potential could be obtained by expanding A_t near the asymptotic boundary $z = 0$ and using the gauge/gravity mapping as,

$$\mu = -\sqrt{\frac{-1}{\int_0^{z_h} dx x^3 e^{-3A(x)} \int_{x_c}^x dx_1 \frac{x_1 e^{-A(x_1)}}{f(x_1)}}} \int_0^{z_h} dx \frac{x e^{-A(x)}}{f(x)}. \quad (2.12)$$

In order to maintain the linear Regge trajectories for the discrete spectrum of the mesons in the boundary theory, the arbitrary function $f(z)$ is considered as the following form,

$$f(z) = e^{-cz^2 - A(z)}, \quad (2.13)$$

Here, the constant $c = 1.16 \text{ GeV}^2$ is fixed by matching the holographic mass spectrum of heavy meson bound states to that of the lowest lying heavy meson states [67]. Using eq. (2.13) in eq. (2.11), the gravity solution is given by

$$\begin{aligned} g(z) &= 1 - \frac{1}{\int_0^{z_h} dx x^3 e^{-3A(x)}} \left[\int_0^z dx x^3 e^{-3A(x)} + \frac{2c\mu^2}{(1 - e^{-cz_h^2})^2} \det \mathcal{G} \right], \\ \phi'(z) &= \sqrt{6(A'^2 - A'' - 2A'/z)}, \\ A_t(z) &= \mu \frac{e^{-cz^2} - e^{-cz_h^2}}{1 - e^{-cz_h^2}}, \\ V(z) &= -\frac{3z^2 g e^{-2A}}{L^2} \left[A'' + A' \left(3A' - \frac{6}{z} + \frac{3g'}{2g} \right) - \frac{1}{z} \left(-\frac{4}{z} + \frac{3g'}{2g} \right) + \frac{g''}{6g} \right] \end{aligned} \quad (2.14)$$

where

$$\det \mathcal{G} = \begin{vmatrix} \int_0^{z_h} dx x^3 e^{-3A(x)} & \int_0^{z_h} dx x^3 e^{-3A(x) - cx^2} \\ \int_{z_h}^z dx x^3 e^{-3A(x)} & \int_{z_h}^z dx x^3 e^{-3A(x) - cx^2} \end{vmatrix}.$$

The Hawking temperature and entropy of the black hole solution of eq. (2.14) are given by,

$$\begin{aligned} T &= \frac{z_h^3 e^{-3A(z_h)}}{4\pi \int_0^{z_h} dx x^3 e^{-3A(x)}} \left[1 + \frac{2c\mu^2 (e^{-cz_h^2} \int_0^{z_h} dx x^3 e^{-3A(x)} - \int_0^{z_h} dx x^3 e^{-3A(x)} e^{-cx^2})}{(1 - e^{-cz_h^2})^2} \right] \\ S &= \frac{L^3 e^{3A(z_h)}}{4G_5 z_h^3}. \end{aligned} \quad (2.15)$$

In holographic QCD models, the appropriate form of the scale factor $A(z)$ is determined to be compatible with certain QCD features like linear Regge trajectories and the QCD phase diagram. In [68]-[70], polynomial functions have been chosen for heavy quarks and in [12], [71] and [72], logarithmic functions of the radial coordinate have been suggested for light quarks. Depending on the arbitrary function $A(z)$, different kinds of phase transitions occur on the gravity side corresponding to different phase transitions in the boundary theories. In [66], a quadratic function for $A(z)$ has been chosen as,

$$A(z) = -\bar{a}z^2, \quad (2.16)$$

for which, there exists a first-order Hawking/Page phase transition from thermal-AdS to black hole which corresponds to the standard confinement/deconfinement phase transition in the dual QCD theory. The parameter $\bar{a} = c/8 \simeq 0.145$ has been fixed such that the critical temperature of the phase transition is around 0.27 GeV at zero chemical potential. By this choice, the analytic solution could be obtained from eq. (2.14) for the dilaton field as,

$$\phi(z) = z\sqrt{3\bar{a}(3 + 2\bar{a}z^2)} + 3\sqrt{\frac{3}{2}} \sinh^{-1} \left[\sqrt{\frac{2\bar{a}}{3}} z \right], \quad (2.17)$$

and the eq. (2.13) gets the following form,

$$f(z) = e^{-(c+\bar{a})z^2}. \quad (2.18)$$

One could also write the near boundary expansion for the dilaton field and the dilaton potential as follows,

$$\begin{aligned} \phi(z) &= 6\sqrt{\bar{a}}z + 2/3\bar{a}^{3/2}z^3 + \dots, \\ V(\phi) &= -\frac{12}{L^2} + \frac{\Delta(\Delta - 4)}{2}\phi^2(z) + \dots, \quad \Delta = 3, \end{aligned} \quad (2.19)$$

where the dimension of the dual operator is $\Delta = 3$ and the dilaton mass is $m^2 = \Delta(\Delta - 4)$. The Hawking temperature in terms of the horizon radius z_h for various values of chemical potential is shown in Fig. 1a. From this figure, one could find that for the stable black hole phase (with small z_h), the slope is negative while, for the unstable thermal AdS phase (with large z_h), the slope is positive. Below a critical chemical potential $\mu_c = 0.673$ GeV, only the unstable branch exists. The stable black hole solution does not exist below a certain minimal temperature T_{min} for each μ which suggests a phase transition from black hole to thermal-AdS as the Hawking temperature decreases. The free energy has been normalized such that the free energy of the thermal-AdS is zero and is shown in Fig. 1b for different values of chemical potential. The phase transition appears in this diagram where the free energy is positive for the unstable branch and becomes negative after some critical temperature T_{crit} along the stable branch. As discussed in ref. [66], this choice of $A(z)$, leads to zero entropy of the quark pair in the dual confined phase. However, in the deconfined phase, the entropy of a quark pair is an increasing function of the pair separation length that saturates to a constant value for large separations as shown in Fig. 2a. This behavior qualitatively resembles the entropy results from lattice QCD of ref. [65]. The entropy of the $q\bar{q}$ pair in terms of temperature in the deconfined phase at large separation is shown in Fig. 2b where a large amount of entropy could be observed near the critical temperature for the quark pair.

The other form of the scale function proposed in ref. [66] is,

$$A(z) = -\frac{3}{4} \ln(az^2 + 1) + \frac{1}{2} \ln(bz^3 + 1) - \frac{3}{4} \ln(az^4 + 1), \quad (2.20)$$

which leads to a first-order phase transition from a small to a large black hole phase as temperature increases. Here, $a = c/9$ and $b = 5c/16$ are determined by demanding the

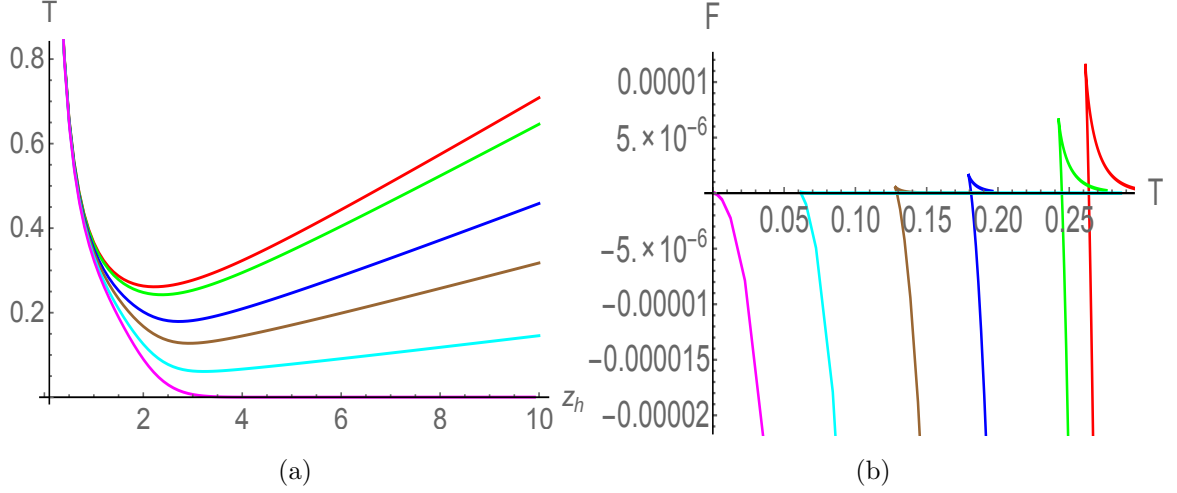


Figure 1: (a) Hawking temperature T as a function of z_h for various values of the chemical potential μ . (b) Normalized free energy F as a function of temperature for various values of the chemical potential μ . Red, green, blue, brown, and cyan curves correspond to $\mu = 0, 0.2, 0.4, 0.5, 0.6$, and 0.673 respectively [66].

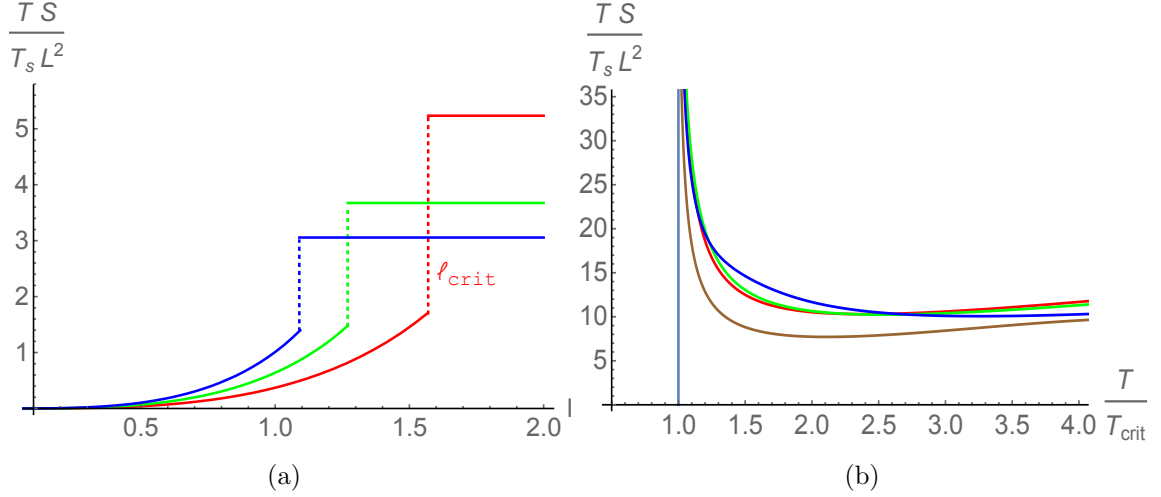


Figure 2: (a) Entropy of the $q\bar{q}$ pair as a function of distance in the deconfined phase for $\mu = 0$. Red, green, and blue curves correspond to $T/T_{crit} = 1.1, 1.2$ and 1.3 respectively. (b) Entropy of the $q\bar{q}$ pair as a function of temperature in the deconfined phase for various values of chemical potential μ . Red, green, blue, and brown curves correspond to $\mu = 0, 0.2, 0.4$ and 0.6 respectively. [66].

transition temperature to be around 0.27 GeV at zero chemical potential. The large black hole phase corresponds to the deconfinement phase of the dual boundary theory, while the small black hole phase corresponds to a *specious-confinement* phase. This phase is called the *specious-confined* since its dual boundary has a very small non-zero expectation value of the Polyakov loop and only shows linear confinement for larger distances at low temperatures therefore, it does not correspond to the confined phase exactly. However, in

the specious-confined phase, the entropy of a $q\bar{q}$ pair in terms of temperature is a slowly varying function at low temperatures and demonstrates rapid increase at high temperatures for different values of chemical potential which is qualitatively similar to the results from lattice QCD where $q\bar{q}$ pair has a large amount of entropy near the critical temperature. The properties of the deconfined phase are similar for both scale functions of eqs. (2.16) and (2.20).

3 Stationary current

In this section, we study the current flow of the holographic QCD model of [66] in the presence of a constant external electric field using the Hashimoto-Oka method of [40].

In holography, for each source on the boundary theory, there exists a corresponding field on the gravity side. Accordingly, the local gauge field in the D7-brane action is dual to the global symmetry of the fermion number in the boundary theory. Therefore, applying an electric field leads to a current flow in the boundary theory as the quarks have an electric charge. In order to have N_f quark flavors in the boundary theory, N_f D7-branes are added to the gravitational background [7]. The D7-branes extend along $AdS_5 \times S^3$ and wrap the S^3 inside a five-dimensional sphere S^5 whose metric is given by,

$$d\Omega_5^2 = L^2(d\theta^2 + \cos^2\theta d\Omega_3^2 + \sin^2\theta d\varphi^2). \quad (3.1)$$

Localization of the D7-brane is parametrized by $\phi = constant$ and the embedding function $\theta(z)$ which is dual to the hypermultiplet mass operator and runs from zero for a massless quark to $\pi/2$ for a quark with large mass.

Here, we are interested in the probe limit for simplicity. In this limit, a finite number of flavors exist in the gauge theory with a large number of color charges so that $N_f \ll N_c$. It means that the small number of probe D7-branes in the gravity side, does not change the gravitational background and one could neglect the back-reaction of the probe brane on the background geometry. This limit is known as the quenched approximation in the lattice gauge theory in which the back-reaction of quarks on the gluon vacuum is neglected and the Wess-Zumino couplings are assumed to be zero [7]. Therefore, the dynamics of the gauge fields living on the probe D7-brane are governed only by the DBI action as,

$$S_{D7} = -\mu_7 \int dt d^3\vec{x} dz d\Omega_3 \sqrt{-\det[g_{ab} + 2\pi\alpha' F_{ab}]}, \quad (3.2)$$

where F_{ab} is the field strength of the gauge field living on the probe brane and μ_7 is the brane tension. Also, $g_{ab} = G_{MN}\partial_a X^M \partial_b X^N$ is the induced metric on the brane where a, b represent the D7-brane coordinates $(t, \vec{x}, z, \Omega_3)$ and M, N represent the background coordinates $(t, \vec{x}, z, \Omega_5)$.

Using eq. (3.2) leads to the following effective Lagrangian in terms of the metric functions and field strengths,

$$\begin{aligned} \mathcal{L} &\propto \int dz (G_{xx}^3 G_{\Omega\Omega}^3 G_{tt} G_{zz})^{1/2} \sqrt{\chi}, \\ \chi &= 1 - \frac{(2\pi\alpha')^2}{G_{xx} G_{tt} G_{zz}} \left(G_{xx} F_{tz}^2 + G_{zz} F_{tx}^2 - G_{tt} F_{zx}^2 \right). \end{aligned} \quad (3.3)$$

From the Lagrangian (3.3), the following equations of motion for the gauge fields are obtained,

$$\begin{aligned} \partial_z \left(\sqrt{\frac{G_{xx}^3}{G_{tt}G_{zz}}} \frac{F_{tz}}{\sqrt{\chi}} \right) = 0 \quad , \quad \partial_t \left(\sqrt{\frac{G_{xx}^3}{G_{tt}G_{zz}}} \frac{F_{tz}}{\sqrt{\chi}} \right) = 0, \\ \partial_z \left(\sqrt{\frac{G_{xx}G_{tt}}{G_{zz}}} \frac{F_{zx}}{\sqrt{\chi}} \right) - \partial_t \left(\sqrt{\frac{G_{xx}G_{zz}}{G_{tt}}} \frac{F_{tx}}{\sqrt{\chi}} \right) = 0, \end{aligned} \quad (3.4)$$

where, we have considered the embedding function $\theta(z) = 0$ in order to have massless hypermultiplets. Therefore, $G_{\Omega\Omega} = L^2$ and we have the flat embedding which always solves the equation of motion derived from the DBI action. For a time-independent electric field, $\partial_t = 0$ and according to the AdS/CFT dictionary, the resulting integration constants of the above equation, corresponding to the electric current flow and the charge density [36]-[38]. Therefore, one can define the dimensionless current flow j and charge density d as,

$$j = \sqrt{\frac{G_{xx}G_{tt}}{G_{zz}}} \frac{2\pi\alpha' F_{zx}}{\sqrt{\chi}}, \quad d = \sqrt{\frac{G_{xx}^3}{G_{tt}G_{zz}}} \frac{2\pi\alpha' F_{tz}}{\sqrt{\chi}}. \quad (3.5)$$

Using these equations to write F_{zx} and F_{tz} in terms of j and d and inserting into the χ definition eq. (3.3) leads to,

$$\chi = \frac{1 - \frac{(2\pi\alpha')^2 E_0^2}{G_{tt}G_{xx}}}{1 + \frac{1}{G_{xx}^3} \left(d^2 - j^2 G_{xx} G_{tt}^{-1} \right)}. \quad (3.6)$$

where $E_0 = F_{tx}$ is the constant external electric field. In order to find the stationary current flow, one can use the reality condition for the D-brane Lagrangian [36]-[38]. Hence, one can write the following equations for the numerator and denominator of χ to change sign simultaneously in a specific radial coordinate $z = z_p$,

$$\left[1 - \frac{(2\pi\alpha')^2 E_0^2}{G_{tt}G_{xx}} \right]_{z=z_p} = 0, \quad (3.7)$$

$$\left[1 + \frac{1}{G_{xx}^3} \left(d^2 - j^2 G_{xx} G_{tt}^{-1} \right) \right]_{z=z_p} = 0. \quad (3.8)$$

From eq. (3.8), we find the following expression for the stationary current $j \equiv j_0$,

$$j_0 = \left[\sqrt{d^2 G_{tt} G_{xx}^{-1} + G_{tt} G_{xx}^2} \right]_{z=z_p}. \quad (3.9)$$

This non-zero current indicates a real effective action for the D7-brane and also an event horizon formation in $z = z_p$. In order to compute the holographic stationary current

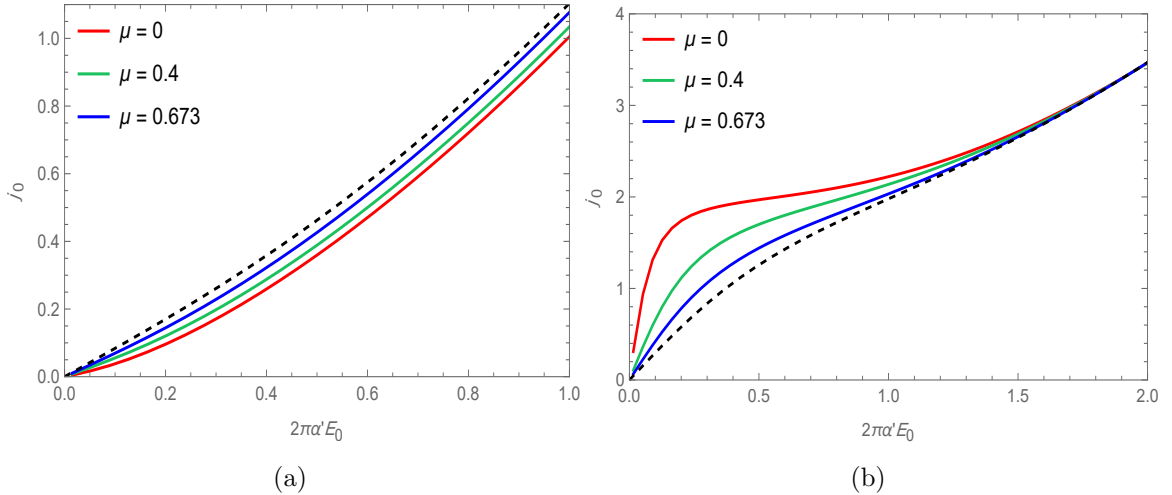


Figure 3: The dimensionless stationary current j_0 in terms of $2\pi\alpha'E_0$ for various values of the chemical potential μ at $T = 0.27$ GeV. Red, green, and blue curves represent $\mu = 0, 0.4,$ and 0.673 respectively. In units GeV and the dashed curves represent the $I - V$ curve for the Hashimoto-Oka model. (a) non-doped case $d = 0$ and (b) doped case $d = 2$.

j_0 , we have obtained z_p numerically from eq. (3.7) and inserted it into eq. (3.9) for different values of the parameters. In our calculation, we have used eq. (2.16) for the scale function which leads to the standard confinement/deconfinement phase transition in the holographic boundary of [66]. The AdS radius is set to 1, and T is the temperature of the initial thermal state given by the Hawking temperature of the black hole solution eq. (2.15).

The holographic current in terms of the rescaled external electric field, $2\pi\alpha'E_0$, is shown in Fig. 3. This figure is depicted for non-doped and doped systems for three different values of chemical potential μ at $T_c = 0.27$ GeV which is the critical temperature of the standard confinement/deconfinement phase transition at zero chemical potential and the minimum temperature for which there always exists the black hole solution for all μ on the gravity side. The dashed curves correspond to the stationary current j_0 in terms of $2\pi\alpha'E_0$ for the massless supersymmetric QCD model which has been called the $I - V$ curve in the Hashimoto-Oka model of ref. [40]. From these figures, we find that our results for the holographic model are less for the non-doped case with $d = 0$ and more for the doped case with $d = 2$ compared to the results from the Hashimoto-Oka model. Likewise, one can observe that in both cases, the curves for $\mu = 0.673$ are closer to the stationary current curves of [40] and for large values of the electric field, all currents converge to the $I - V$ curves of the Hashimoto-Oka model.

Also, the stationary current in terms of the rescaled temperature T/T_c is depicted in Fig. 4 for $E_0 = 0.5$ and three different values of chemical potential μ . For each value of μ , the corresponding curve starts from a critical temperature T_{crit} which is determined by the free energy diagram of Fig. 1b. A non-trivial behavior could be found at lower temperatures accessible for larger μ , where the current is larger (less) than the Hashimoto-Oka model for $d = 0$ ($d = 2$) case. A similar behavior to the $j_0 - E_0$ figures could be observed from

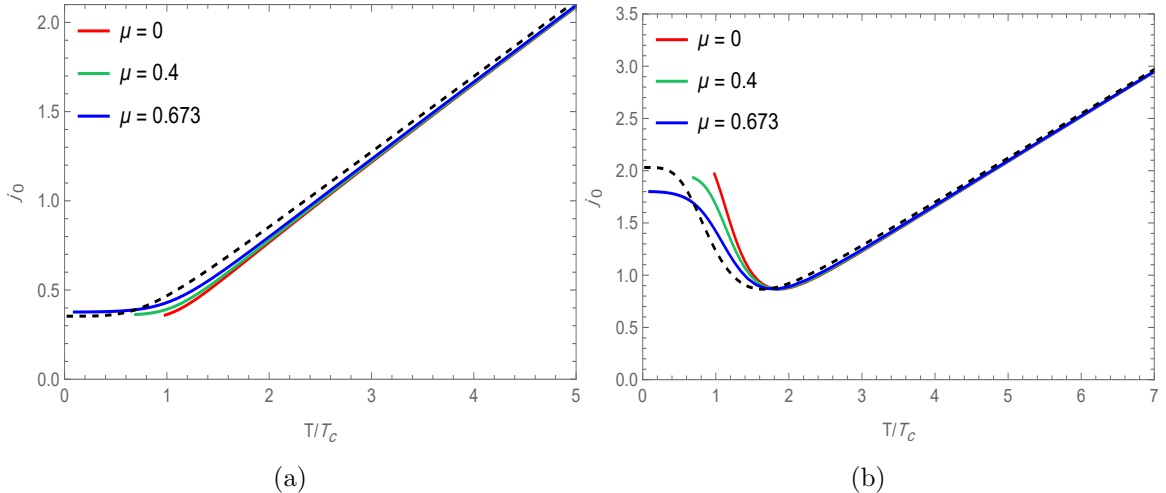


Figure 4: The dimensionless stationary current j_0 versus T for various values of the chemical potential μ at $E_0 = 0.5$ GeV. Red, green, and blue curves represent $\mu = 0, 0.4,$ and 0.673 respectively. In units GeV and the dashed curves represent the $I-V$ curve results of the Hashimoto-Oka model. (a) non-doped case $d = 0$ and (b) doped case $d = 2$.

these diagrams for $T \gtrsim 0.2$, and all currents converge to the Hashimoto-Oka model curve at high temperatures.

4 Time dependent current

In this section, we are going to investigate the dynamical response of the holographic QCD model to an external time-dependent electric field. In this phenomenon, the system experiences a time-dependent energy injection, which gives rise to a time-dependent current flow $j(t)$ in the boundary theory. The initial state is at a finite temperature and after a while, the system relaxes into the final steady state current j_0 corresponding to the final amount of the electric field. For this purpose, we use two different relaxation time scales, equilibration time and thermalization time.

The first time scale is the equilibration time, t_{eq} , which is defined as the first time that the time-dependent response (which is the electric current in our case) reaches its final stationary value with 5% uncertainty and remains within this regime afterward [29]. Using this time scale enables us to find out how the energy injection rate affects the system evolution and relaxation as it depends on the quench speed. Here, we use the following time-dependent error parameter,

$$\delta(t) = \frac{j(t) - j_0}{j_0}, \quad (4.1)$$

therefore, $\delta(t_{eq}) < 0.05$ for all $t > t_{eq}$.

The second time scale is the thermalization time for which, the time-dependent current relaxes to its final steady-state value j_0 corresponding to the electric field's final value. On the gravity side, it corresponds to the time in which the apparent horizon approaches the

event horizon on the D7-brane at late times. Unlike the equilibration time, this time scale does not depend on the energy injection rate and only depends on the late-time effective temperature of the D7-brane after the quench and is argued to have a universal scaling behavior of the following form [40],

$$t_{th} \propto \frac{1}{T_{eff}^\infty}, \quad (4.2)$$

where T_{eff}^∞ is the asymptotic value of the effective temperature that is felt by the fundamental matter in the quark-gluon plasma due to the pair creation in the presence of an external electric field [62].

In order to calculate the equilibration time, we have to find the time-dependent current for different parameters. For this purpose, we use the Lagrangian (3.3) to obtain the equations of motion for the gauge field A_x as follows,

$$\begin{aligned} \partial_z \left(\sqrt{\frac{G_{xx}G_{tt}}{G_{zz}}} \frac{F_{zx}}{\sqrt{\chi}} \right) - \partial_t \left(\sqrt{\frac{G_{xx}G_{zz}}{G_{tt}}} \frac{F_{tx}}{\sqrt{\chi}} \right) &= 0, \\ \chi &= 1 - \frac{(2\pi\alpha')^2}{G_{xx}G_{tt}G_{zz}} \left(G_{zz}F_{tx}^2 - G_{tt}F_{zx}^2 \right), \end{aligned} \quad (4.3)$$

where we have used the gauge choice $A_z = 0$ and assumed the charge density d equal to zero. In order to have a time-dependent electric current, we consider the following ansatz for the gauge field [40],

$$\begin{aligned} A_x &= - \int^t E(s)ds + h(t, z), \\ E(t) &= \frac{E_0}{2} \left(1 + \tanh\left(\frac{t}{k}\right) \right), \end{aligned} \quad (4.4)$$

where $E(t)$ a time-dependent electric field in the x direction that increases from zero at t_0 to its final value E_0 . The rate of energy injection to the system is controlled by the characteristic time scale k . Using the ansatz of eq. (4.4), the equation of motion (4.3) would be a second-order nonlinear equation in both t and z for $h(t, z)$. Near boundary expansion of the equation of motion for A_x , leads to $h(z) \simeq b + az^2 + O(z^4)$. According to the AdS/CFT dictionary, the sub-leading term a is proportional to the expectation value of the dual operator which translates to the current density of the boundary theory (the leading source term b is a constant that sets to zero) [36]. Therefore, the time-dependent current in the boundary theory is proportional to the second derivative of $h(t, z)$ with respect to z at the boundary,

$$j(t) \propto \partial_z^2 h(t, z = 0). \quad (4.5)$$

In order to obtain the time-dependent electric current, we use the boundary conditions $h(t, z = 0) = \partial_z h(t, z = 0) = 0$ and initial conditions $h(t_0, z) = \partial_z h(t_0, z) = 0$ to solve the equation of motion numerically for different parameters such as the final value of the electric field, chemical potential, temperature, and the characteristic time scale.

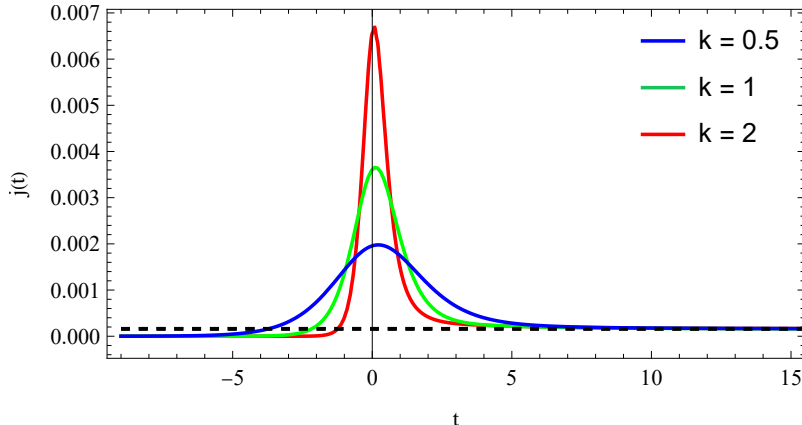


Figure 5: (Color online) The time-dependent current $j(t)$ versus t for $2\pi\alpha'E_0 = 0.001$ and $T = 0.03\text{GeV}$ and $\mu = \mu_c$. Blue, green, and red curves correspond to $k = 0.5, 1,$ and 2 respectively. The dashed line is the static current j_0 .

In the following calculations, T is the temperature of the initial thermal state given by the Hawking temperature eq. (2.15), and we have set the AdS radius equal to 1 for numerical calculations. Also, $\mu_c = 0.673$ and $T_c = 0.27$ (in GeV units) represent the critical chemical potential and critical temperature.

In Fig. 5 the time-dependent currents are shown for three different values of the characteristic time scale k . This figure is depicted for the lowest temperature of the holographic QCD model $T = 0.03$ GeV associated with $\mu = \mu_c$ and $2\pi\alpha'E_0 = 0.001$. One can find that each current flow increases from zero to a maximum value and after a while, relaxes to the black dashed line j_0 defined by eq. (3.9). As mentioned before, the characteristic time scale k defines the energy injection rate, and increasing k leads to higher peaks in the current flow and lower equilibration times.

The rescaled equilibration time $T_c t_{eq}$ versus the chemical potential ratio μ/μ_c is plotted in Fig. 6 for $k = 0.25$ and three different values of temperature. From this figure, one could observe that increasing chemical potential leads to increasing the rescaled equilibration time, and also, higher temperatures give rise to lower equilibration time.

Next, we are going to analyze the thermal quench in two different regimes of the characteristic time scale k during which the electric field changes from zero to a constant value. The fast quenches with $k < 1$ are more rapid quenches and result in faster energy injection and equilibration, while the slow quench is the opposite limit with large k [30]-[34].

The equilibration time for the slow quench regime is displayed in Fig. 7a for $2\pi\alpha'E_0 = 0.001$. In this case, the electric field changes slowly over a long period, leading to an adiabatic response as the system has enough time to adjust to the energy injection and relax. From this figure, could find that for smaller values of k , the points corresponding to different temperatures are widely separated, while increasing the characteristic time scale leads to decreasing the rescaled equilibration time, and in large k limit, the equilibration time scales as $t_{eq} \sim 1/k^2$ and the curves of different temperatures coincide. This could be regarded as a consequence of the zero entropy production in the adiabatic limit, analog to

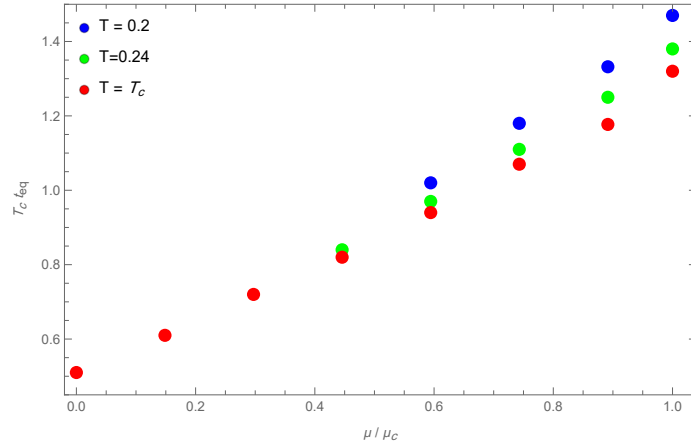


Figure 6: The rescaled equilibration time in terms of μ/μ_c for $2\pi\alpha'E_0 = 0.001$. Here, $k = 0.25$ and blue, green and red lines correspond to $T = 0.2$, 0.24 , and 0.27 GeV respectively.

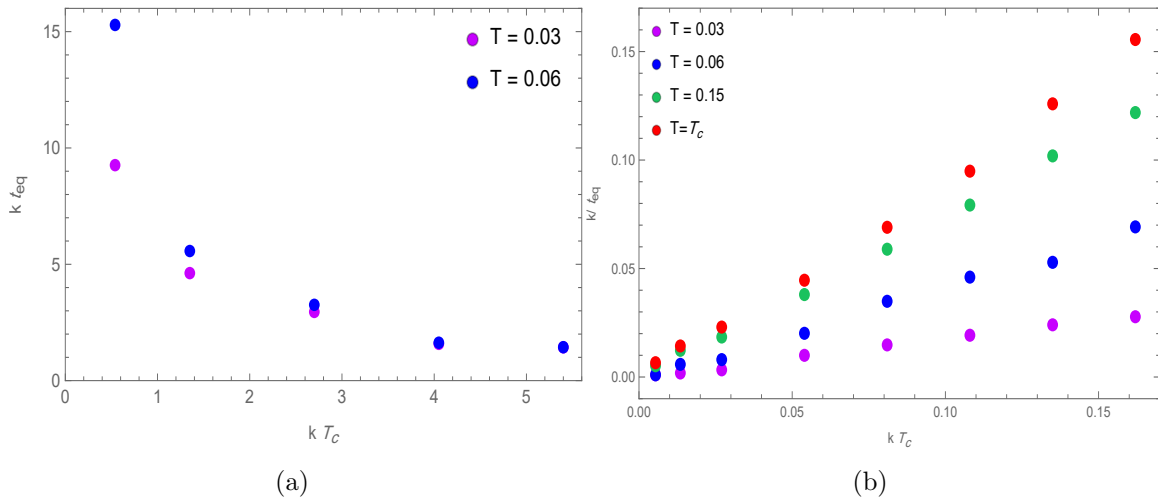


Figure 7: (Color online) Slow and fast quenches for $2\pi\alpha'E_0 = 0.001$. (a) Slow quench regime: $k^{-1}t_{eq}$ with respect to k for $T = 0.03$ and 0.06 (in GeV units). (b) Fast quench regime: $k t_{eq}^{-1}$ with respect to k for $T = 0.03, 0.06, 0.15$, and T_c (in GeV units).

the slow quench regime behavior found in [30].

In Fig. 7b, the rescaled equilibration time $k t_{eq}^{-1}$ is plotted with respect to k for $2\pi\alpha'E_0 = 0.001$ at different temperatures. One could observe that decreasing k leads to a universal behavior independent of temperature in which all data converge to a single point at the $k \rightarrow 0$ limit. Also, for small k , the slope of the line connecting the points of each T is a constant proportional to the inverse of the temperature, indicating that in the fast quench regime, $t_{eq} \sim 1/T$ and increasing temperature leads to decreasing the equilibration time. It is consistent with the universal scaling behavior found in [30], where the relaxation time is set by the thermal time scale for fast quenches, regardless of the quenching rate.

The rescaled equilibration time $T_c t_{eq}$ in terms of the dimensionless parameter $2\pi\alpha'E_0$

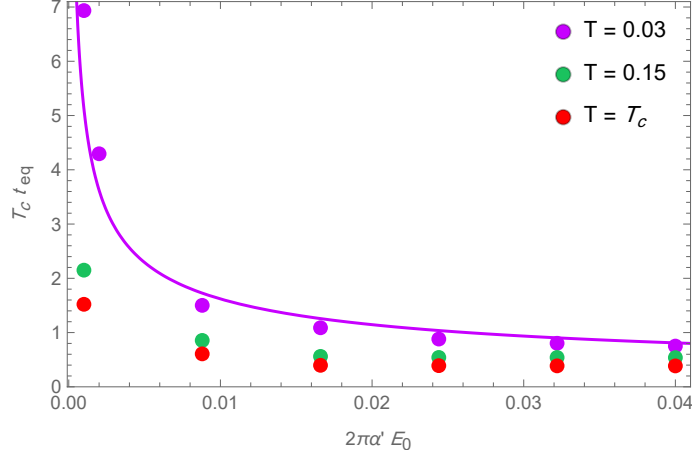


Figure 8: (Color online) The rescaled equilibration time versus $2\pi\alpha'E_0$ for $k = 0.25$ and $\mu = \mu_c$. The purple, green, and red points represent data for $T = 0.03$, 0.15 , and T_c , respectively. The purple curve is a polynomial fit to $T = 0.03$ data.

is plotted in Fig. 8 for $\mu = \mu_c$ and $k = 0.25$ and different temperatures. The purple curve is a polynomial fitting to the lowest temperature data and has the following form,

$$t_{eq} \simeq 0.6 (2\pi\alpha'E_0)^{-1/2}, \quad (4.6)$$

From this figure, one can observe that for larger electric field values, the equilibration time is less sensitive to temperature, and all curves approach the purple curve. Also, from Figs. 8 and 6, one could find that the equilibration time decreases by increasing temperature as well as decreasing chemical potential, and therefore, eq. (4.6) could be regarded as the upper bound of the equilibration time of the holographic QCD mode. One could compare eq. (4.6) with the thermalization time obtained in the Hashimoto-Oka model (in units of $2\pi\alpha'$) and find the value $t_{eq} \sim 0.4 \text{ fm}/c$ for the equilibration time in the presence of an external electric field of order 10^4 MeV^2 ¹. This value is comparable with the isotropization time of the far-from-equilibrium non-isotropic plasma studied in [28], despite the different geometries, sources, and computational methods. In [28], a time-dependent shear (similar to $E(t)$ in eq. (4.4)) is considered in the geometry and the isotropization time is considered as the time when the transverse and longitudinal pressures deviate from their final values by less than 10% and for transition times less than or equal to 2 the isotropization time is estimated to be $0.5 \text{ fm}/c$ for $T = 0.35 \text{ GeV}$.

Finally, the rescaled thermalization time in terms of $2\pi\alpha'E_0$ is plotted in Fig. 9 for two different values of chemical potential and different temperatures. We have used eq. (4.2), where $1/T_{eff}^\infty$ is regarded as the thermalization time scale independent of the quench speed. From this figure, one could find that the thermalization time decreases with increasing temperature and electric field strength. Figure 9a represents data for $\mu = \mu_c$ where thermalization time decreases from about $0.7 \text{ fm}/c$ to $0.6 \text{ fm}/c$ as temperature increases from

¹Strong electromagnetic fields expected to be produced in heavy-ion collisions [73] with the magnitude of order 10^4 MeV^2 (see for example, [74])

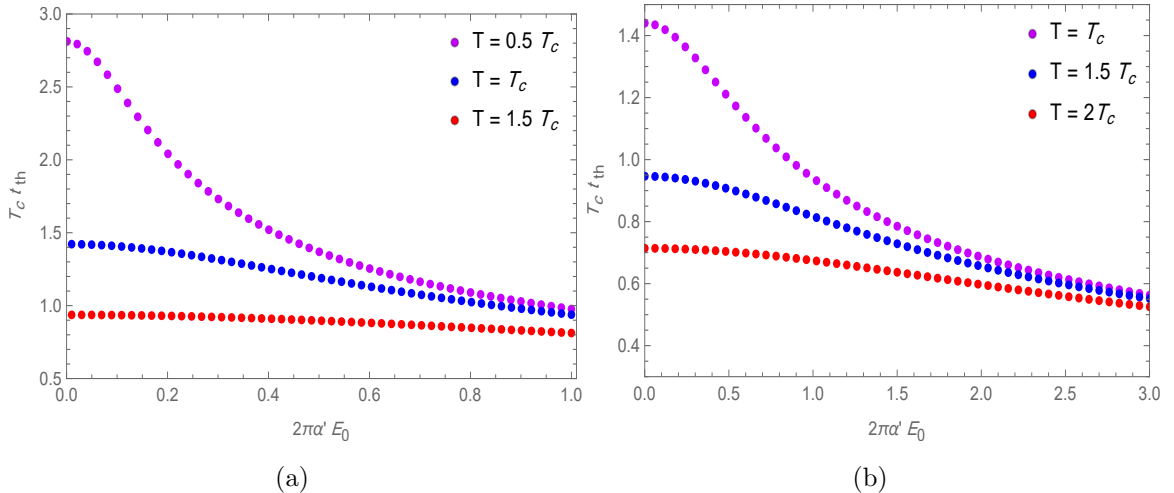


Figure 9: (Color online) The rescaled thermalization time in terms of the electric field strength for different temperatures. (a) $\mu = \mu_c$ and purple, blue and red dots represent data for $T = 0.5 T_c$, T_c and $1.5 T_c$ respectively. (b) $\mu = 0$ and purple, blue and red dots represent data for T_c , $1.5 T_c$ and $2 T_c$.

$0.5 T_c$ to $1.5 T_c$. Also, figure 9b represents data for $\mu = 0$ and exhibits a decrease of thermalization time from about $0.7 \text{ fm}/c$ to $0.5 \text{ fm}/c$ as temperature increases with $2\pi\alpha'E_0$ from T_c to $2 T_c$. The above values are obtained for $2\pi\alpha'E_0 = 1$, $T_c = 0.27 \text{ GeV}$, and $1 \text{ fm}/c \simeq 5 \text{ GeV}^{-1}$. On the other hand, the thermalization time of the charm quarks is estimated to be decreasing in temperature and lying in the range $4 - 6 \text{ fm}/c$ for temperatures $3T_c$ to T_c [23] and [24]. Also, at any temperature, the thermalization time of heavy quarks is larger than the thermalization time of light quarks by a factor M/T where M is the mass of heavy quark (see [26] for example). Therefore, our results are qualitatively in agreement with the thermalization time computed in the literature.

5 Conclusion

In this paper, we have investigated the equilibration and thermalization times of a massless quark in the presence of an external electric field by using the gauge/gravity duality. Our results demonstrate that for a strong electric field $E_0 = 10^4 \text{ MeV}^2$, the equilibration time would be about $0.4 \text{ fm}/c$ which is comparable to the isotropization time obtained in [28] despite different holographic models, sources, and implemented methods. This could be regarded as the characteristics of thermal quenches for the strongly coupled gauge theories reported in the literature for the fast quenches where the equilibration times for all temperatures converge to a single value for abrupt quenches.

The thermalization time of the quark-gluon plasma has also been calculated for the holographic QCD model using the inverse of the effective temperature for zero and the critical chemical potential. Our results are qualitatively in agreement with those computed using both phenomenological and holographic models, as the equilibration and thermalization times have $O(1)$ in magnitude as well as evident temperature dependency. The results

for the equilibration and thermalization time scales indicate that, in the presence of an external electric field, the quark-gluon plasma equilibrates first and then thermalizes.

References

- [1] J. M. Maldacena, “The Large N limit of superconformal field theories and supergravity,” *Int. J. Theor. Phys.* **38**, 1113 (1999) [*Adv. Theor. Math. Phys.* **2**, 231 (1998)] [hep-th/9711200].
- [2] E. Witten, “Anti-de Sitter space and holography,” *Adv. Theor. Math. Phys.* **2**, 253 (1998) [hep-th/9802150].
- [3] S. S. Gubser, I. R. Klebanov and A. M. Polyakov, “Gauge theory correlators from noncritical string theory,” *Phys. Lett. B* **428**, 105 (1998) [hep-th/9802109].
- [4] O. Aharony, S. S. Gubser, J. M. Maldacena, H. Ooguri and Y. Oz, “Large N field theories, string theory and gravity,” *Phys. Rept.* **323**, 183 (2000) [hep-th/9905111].
- [5] J. Casalderrey-Solana, H. Liu, D. Mateos, K. Rajagopal and U. A. Wiedemann, “Gauge/String Duality, Hot QCD and Heavy Ion Collisions,” book:*Gauge/String Duality, Hot QCD and Heavy Ion Collisions*. Cambridge, UK: Cambridge University Press, 2014 [arXiv:1101.0618 [hep-th]].
- [6] J. Polchinski and M. J. Strassler, “The String dual of a confining four-dimensional gauge theory,” hep-th/0003136.
- [7] A. Karch and E. Katz, “Adding flavor to AdS / CFT,” *JHEP* **0206**, 043 (2002) [hep-th/0205236].
- [8] T. Sakai and S. Sugimoto, “Low energy hadron physics in holographic QCD,” *Prog. Theor. Phys.* **113**, 843 (2005) [hep-th/0412141].
- [9] E. Witten, “Anti-de Sitter space, thermal phase transition, and confinement in gauge theories,” *Adv. Theor. Math. Phys.* **2** (1998) 505 [hep-th/9803131].
- [10] M. Kruczenski, D. Mateos, R. C. Myers and D. J. Winters, “Towards a holographic dual of large N_c QCD,” *JHEP* **0405** (2004) 041 [hep-th/0311270].
- [11] J. Erlich, E. Katz, D. T. Son and M. A. Stephanov, “QCD and a holographic model of hadrons,” *Phys. Rev. Lett.* **95** (2005) 261602 [hep-ph/0501128].
- [12] U. Gursoy, E. Kiritsis, L. Mazzanti, G. Michalogiorgakis and F. Nitti, *Lect. Notes Phys.* **828**, 79-146 (2011) doi:10.1007/978-3-642-04864-7_4 [arXiv:1006.5461 [hep-th]].
- [13] U. Gursoy, E. Kiritsis, L. Mazzanti and F. Nitti, “Improved Holographic Yang-Mills at Finite Temperature: Comparison with Data,” *Nucl. Phys. B* **820**, 148 (2009) [arXiv:0903.2859 [hep-th]].
- [14] T. Alho, M. Järvinen, K. Kajantie, E. Kiritsis, C. Rosen and K. Tuominen, “A holographic model for QCD in the Veneziano limit at finite temperature and density,” *JHEP* **1404**, 124 (2014) Erratum: [*JHEP* **1502**, 033 (2015)] [arXiv:1312.5199 [hep-ph]].
- [15] C. P. Herzog, “A Holographic Prediction of the Deconfinement Temperature,” *Phys. Rev. Lett.* **98** (2007) 091601 [hep-th/0608151].
- [16] A. Karch, E. Katz, D. T. Son and M. A. Stephanov, “Linear confinement and AdS/QCD,” *Phys. Rev. D* **74** (2006) 015005 [hep-ph/0602229].

- [17] P. Colangelo, F. Giannuzzi, S. Nicotri and V. Tangorra, “Temperature and quark density effects on the chiral condensate: An AdS/QCD study,” *Eur. Phys. J. C* **72** (2012) 2096 [arXiv:1112.4402 [hep-ph]].
- [18] T. Gherghetta, J. I. Kapusta and T. M. Kelley, “Chiral symmetry breaking in the soft-wall AdS/QCD model,” *Phys. Rev. D* **79** (2009) 076003 [arXiv:0902.1998 [hep-ph]].
- [19] M. Panero, “Thermodynamics of the QCD plasma and the large-N limit,” *Phys. Rev. Lett.* **103**, 232001 (2009) [arXiv:0907.3719 [hep-lat]].
- [20] D. Banerjee, S. Datta, R. Gavai and P. Majumdar, *Phys. Rev. D* **85**, 014510 (2012) doi:10.1103/PhysRevD.85.014510 [arXiv:1109.5738 [hep-lat]].
- [21] O. Kaczmarek, *Nucl. Phys. A* **931**, 633-637 (2014) doi:10.1016/j.nuclphysa.2014.09.031 [arXiv:1409.3724 [hep-lat]].
- [22] U. W. Heinz, *AIP Conf. Proc.* **739**, no.1, 163-180 (2004) doi:10.1063/1.1843595 [arXiv:nucl-th/0407067 [nucl-th]].
- [23] S. K. Das, F. Scardina, S. Plumari and V. Greco, *Phys. Lett. B* **747**, 260-264 (2015) doi:10.1016/j.physletb.2015.06.003 [arXiv:1502.03757 [nucl-th]].
- [24] F. Scardina, S. K. Das, V. Minissale, S. Plumari and V. Greco, *Phys. Rev. C* **96**, no.4, 044905 (2017) doi:10.1103/PhysRevC.96.044905 [arXiv:1707.05452 [nucl-th]].
- [25] H. van Hees and R. Rapp, *Phys. Rev. C* **71**, 034907 (2005) doi:10.1103/PhysRevC.71.034907 [arXiv:nucl-th/0412015 [nucl-th]].
- [26] G. D. Moore and D. Teaney, *Phys. Rev. C* **71**, 064904 (2005) doi:10.1103/PhysRevC.71.064904 [arXiv:hep-ph/0412346 [hep-ph]].
- [27] S. S. Gubser, *Phys. Rev. D* **76**, 126003 (2007) doi:10.1103/PhysRevD.76.126003 [arXiv:hep-th/0611272 [hep-th]].
- [28] P. M. Chesler and L. G. Yaffe, *Phys. Rev. Lett.* **102**, 211601 (2009) doi:10.1103/PhysRevLett.102.211601 [arXiv:0812.2053 [hep-th]].
- [29] A. Buchel, L. Lehner and R. C. Myers, “Thermal quenches in $N=2^*$ plasmas,” *JHEP* **08**, 049 (2012) [arXiv:1206.6785 [hep-th]].
- [30] A. Buchel, R. C. Myers and A. van Niekerk, “Nonlocal probes of thermalization in holographic quenches with spectral methods,” *JHEP* **02**, 017 (2015) [erratum: *JHEP* **07**, 137 (2015)] [arXiv:1410.6201 [hep-th]].
- [31] A. Buchel, R. C. Myers and A. van Niekerk, “Universality of Abrupt Holographic Quenches,” *Phys. Rev. Lett.* **111**, 201602 (2013) [arXiv:1307.4740 [hep-th]].
- [32] A. Buchel, L. Lehner, R. C. Myers and A. van Niekerk, “Quantum quenches of holographic plasmas,” *JHEP* **05**, 067 (2013) [arXiv:1302.2924 [hep-th]].
- [33] S. R. Das, D. A. Galante and R. C. Myers, “Universal scaling in fast quantum quenches in conformal field theories,” *Phys. Rev. Lett.* **112**, 171601 (2014) [arXiv:1401.0560 [hep-th]].
- [34] S. R. Das, D. A. Galante and R. C. Myers, “Universality in fast quantum quenches,” *JHEP* **02**, 167 (2015) [arXiv:1411.7710 [hep-th]].
- [35] E. Caceres, A. Kundu, J. F. Pedraza and D. L. Yang, “Weak Field Collapse in AdS: Introducing a Charge Density,” *JHEP* **06**, 111 (2015) [arXiv:1411.1744 [hep-th]].

- [36] A. Karch and A. O’Bannon, “Metallic AdS/CFT,” *JHEP* **09**, 024 (2007) [arXiv:0705.3870 [hep-th]].
- [37] A. Karch and A. O’Bannon, “Holographic thermodynamics at finite baryon density: Some exact results,” *JHEP* **11**, 074 (2007) [arXiv:0709.0570 [hep-th]].
- [38] J. Erdmenger, R. Meyer and J. P. Shock, “AdS/CFT with flavour in electric and magnetic Kalb-Ramond fields,” *JHEP* **12**, 091 (2007) [arXiv:0709.1551 [hep-th]].
- [39] K. Hashimoto, T. Oka and A. Sonoda, “Electromagnetic instability in holographic QCD,” *JHEP* **06**, 001 (2015) doi:10.1007/JHEP06(2015)001 [arXiv:1412.4254 [hep-th]].
- [40] K. Hashimoto and T. Oka, “Vacuum Instability in Electric Fields via AdS/CFT: Euler-Heisenberg Lagrangian and Planckian Thermalization,” *JHEP* **1310**, 116 (2013) [arXiv:1307.7423].
- [41] K. Hashimoto, S. Kinoshita, K. Murata and T. Oka, “Electric Field Quench in AdS/CFT,” *JHEP* **09**, 126 (2014) [arXiv:1407.0798 [hep-th]].
- [42] S. Amiri-Sharifi, H. R. Sepangi and M. Ali-Akbari, “Electric Field Quench, Equilibration and Universal Behavior,” *Phys. Rev. D* **91**, 126007 (2015) [arXiv:1504.03559 [hep-th]].
- [43] M. Ali-Akbari and F. Charmchi, “Holographic Equilibration under External Dynamical Electric Field,” *Phys. Lett. B* **773**, 271-276 (2017) [arXiv:1612.09098 [hep-th]].
- [44] M. Ali-Akbari, F. Charmchi, H. Ebrahim and L. Shahkarami, “Various Time-Scales of Relaxation,” *Phys. Rev. D* **94**, no.4, 046008 (2016) [arXiv:1602.07903 [hep-th]].
- [45] H. Ebrahim, S. Heshmatian and M. Ali-Akbari, “Thermal quench at finite ’t Hooft coupling,” *Nucl. Phys. B* **904**, 527-537 (2016) [arXiv:1510.07974 [hep-th]].
- [46] V. Skokov, A. Y. Illarionov and V. Toneev, “Estimate of the magnetic field strength in heavy-ion collisions,” *Int. J. Mod. Phys. A* **24**, 5925-5932 (2009) [arXiv:0907.1396 [nucl-th]].
- [47] V. Voronyuk, V. D. Toneev, W. Cassing, E. L. Bratkovskaya, V. P. Konchakovski and S. A. Voloshin, “(Electro-)Magnetic field evolution in relativistic heavy-ion collisions,” *Phys. Rev. C* **83**, 054911 (2011) doi:10.1103/PhysRevC.83.054911 [arXiv:1103.4239 [nucl-th]].
- [48] J. S. Schwinger, “On gauge invariance and vacuum polarization,” *Phys. Rev.* **82**, 664-679 (1951)
- [49] I. K. Affleck, O. Alvarez and N. S. Manton, “Pair Production at Strong Coupling in Weak External Fields,” *Nucl. Phys. B* **197**, 509-519 (1982)
- [50] G. W. Semenoff and K. Zarembo, “Holographic Schwinger Effect,” *Phys. Rev. Lett.* **107**, 171601 (2011) [arXiv:1109.2920 [hep-th]].
- [51] Y. Sato and K. Yoshida, “Potential Analysis in Holographic Schwinger Effect,” *JHEP* **08**, 002 (2013) [arXiv:1304.7917 [hep-th]].
- [52] Y. Sato and K. Yoshida, “Universal aspects of holographic Schwinger effect in general backgrounds,” *JHEP* **12**, 051 (2013) [arXiv:1309.4629 [hep-th]].
- [53] Y. Sato and K. Yoshida, “Holographic description of the Schwinger effect in electric and magnetic fields,” *JHEP* **04**, 111 (2013) [arXiv:1303.0112 [hep-th]].
- [54] S. Bolognesi, F. Kiefer and E. Rabinovici, “Comments on Critical Electric and Magnetic Fields from Holography,” *JHEP* **01**, 174 (2013) [arXiv:1210.4170 [hep-th]].

- [55] Y. Sato and K. Yoshida, “Holographic Schwinger effect in confining phase,” *JHEP* **09**, 134 (2013) [arXiv:1306.5512 [hep-th]].
- [56] D. Kawai, Y. Sato and K. Yoshida, “Schwinger pair production rate in confining theories via holography,” *Phys. Rev. D* **89**, no.10, 101901 (2014) [arXiv:1312.4341 [hep-th]].
- [57] W. Fischler, P. H. Nguyen, J. F. Pedraza and W. Tangarife, “Holographic Schwinger effect in de Sitter space,” *Phys. Rev. D* **91**, no.8, 086015 (2015) [arXiv:1411.1787 [hep-th]].
- [58] L. Shahkarami, “Magnetized Einstein–Maxwell-dilaton model under an external electric field,” *Eur. Phys. J. C* **82**, no.1, 33 (2022) [arXiv:2111.04813 [hep-th]].
- [59] M. Ghodrati, “Schwinger Effect and Entanglement Entropy in Confining Geometries,” *Phys. Rev. D* **92**, no.6, 065015 (2015) [arXiv:1506.08557 [hep-th]].
- [60] S. J. Zhang and E. Abdalla, “Holographic Schwinger effect in a confining background with Gauss–Bonnet corrections,” *Gen. Rel. Grav.* **48**, no.5, 60 (2016) [arXiv:1508.03364 [hep-th]].
- [61] D. Kawai, Y. Sato and K. Yoshida, “A holographic description of the Schwinger effect in a confining gauge theory,” *Int. J. Mod. Phys. A* **30**, no.11, 1530026 (2015) [arXiv:1504.00459 [hep-th]].
- [62] K. Y. Kim, J. P. Shock and J. Tarrio, *JHEP* **06**, 017 (2011) doi:10.1007/JHEP06(2011)017 [arXiv:1103.4581 [hep-th]].
- [63] A. Adare *et al.* [PHENIX], “ J/ψ Production vs Centrality, Transverse Momentum, and Rapidity in Au+Au Collisions at $\sqrt{s_{NN}} = 200$ GeV,” *Phys. Rev. Lett.* **98**, 232301 (2007) [arXiv:nucl-ex/0611020 [nucl-ex]].
- [64] B. B. Abelev *et al.* [ALICE], “Centrality, rapidity and transverse momentum dependence of J/ψ suppression in Pb-Pb collisions at $\sqrt{s_{NN}}=2.76$ TeV,” *Phys. Lett. B* **734**, 314-327 (2014) [arXiv:1311.0214 [nucl-ex]].
- [65] O. Kaczmarek and F. Zantow, *PoS LAT2005*, 192 (2006) doi:10.22323/1.020.0192 [arXiv:hep-lat/0510094 [hep-lat]].
- [66] D. Dudal and S. Mahapatra, “Thermal entropy of a quark-antiquark pair above and below deconfinement from a dynamical holographic QCD model,” *Phys. Rev. D* **96**, no.12, 126010 (2017) [arXiv:1708.06995 [hep-th]].
- [67] S. He, S. Y. Wu, Y. Yang and P. H. Yuan, *JHEP* **04**, 093 (2013) doi:10.1007/JHEP04(2013)093 [arXiv:1301.0385 [hep-th]].
- [68] O. Andreev and V. I. Zakharov, *JHEP* **04**, 100 (2007) doi:10.1088/1126-6708/2007/04/100 [arXiv:hep-ph/0611304 [hep-ph]].
- [69] Y. Yang and P. H. Yuan, *JHEP* **12**, 161 (2015) doi:10.1007/JHEP12(2015)161 [arXiv:1506.05930 [hep-th]].
- [70] I. Aref’eva and K. Rannu, *JHEP* **05**, 206 (2018) doi:10.1007/JHEP05(2018)206 [arXiv:1802.05652 [hep-th]].
- [71] M. W. Li, Y. Yang and P. H. Yuan, *Phys. Rev. D* **96**, no.6, 066013 (2017) doi:10.1103/PhysRevD.96.066013 [arXiv:1703.09184 [hep-th]].
- [72] I. Y. Aref’eva, K. Rannu and P. Slepov, *JHEP* **06**, 090 (2021) doi:10.1007/JHEP06(2021)090 [arXiv:2009.05562 [hep-th]].
- [73] D. E. Kharzeev, L. D. McLerran and H. J. Warringa, *Nucl. Phys. A* **803**, 227-253 (2008) doi:10.1016/j.nuclphysa.2008.02.298 [arXiv:0711.0950 [hep-ph]].

- [74] V. Voronyuk, V. D. Toneev, W. Cassing, E. L. Bratkovskaya, V. P. Konchakovski and S. A. Voloshin, *Phys. Rev. C* **83**, 054911 (2011) doi:10.1103/PhysRevC.83.054911 [arXiv:1103.4239 [nucl-th]].